Improving astrophysical parameter estimation via offline noise subtraction for Advanced LIGO

J. C. Driggers,[1,*] S. Vitale,[2] A. P. Lundgren,[3] M. Evans,[2] K. Kawabe,[1] S. E. Dwyer,[1] K. Izumi,[1] R. M. S. Schofield,[4] A. Effler,[5] D. Sigg,[1] P. Fritschel,[2] M. Drago,[3] A. Nitz,[3] B. P. Abbott,[6] R. Abbott,[6] T. D. Abbott,[7] C. Adams,[5] R. X. Adhikari,[6] V. B. Adya,[3] A. Ananyeva,[6] S. Appert,[6] K. Arai,[6] S. M. Aston,[5] C. Austin,[7] S. W. Ballmer,[8] D. Barker,[1] B. Barr,[9] L. Barsotti,[2] J. Bartlett,[1] I. Bartos,[10] J. C. Batch,[1] A. S. Bell,[9] J. Betzwieser,[5] G. Billingsley,[6] J. Birch,[5] S. Biscans,[2] C. D. Blair,[5] R. M. Blair,[1] R. Bork,[6] A. F. Brooks,[6] H. Cao,[11] G. Ciani,[10] F. Clara,[1] S. J. Cooper,[12] P. Corban,[5] S. T. Countryman,[13] P. B. Covas,[14] M. J. Cowart,[5] D. C. Coyne,[6] A. Cumming,[9] L. Cunningham,[9] K. Danzmann,[3,15] C. F. Da Silva Costa,[10] E. J. Daw,[16] D. DeBra,[17] R. DeSalvo,[18] K. L. Dooley,[19,20] S. Doravari,[3,15] T. B. Edo,[16] T. Etzel,[6] T. M. Evans,[5] H. Fair,[8] A. Fernandez-Galiana,[2] E. C. Ferreira,[21] R. P. Fisher,[8] H. Fong,[22] R. Frey,[4] V. V. Frolov,[5] P. Fulda,[10] M. Fyffe,[5] B. Gateley,[1] J. A. Giaime,[7,5] K. D. Giardina,[5] E. Goetz,[1] R. Goetz,[10] S. Gras,[2] C. Gray,[1] H. Grote,[19] K. E. Gushwa,[6] E. K. Gustafson,[6] R. Gustafson,[23] E. D. Hall,[2] G. Hammond,[9] J. Hanks,[1] J. Hanson,[5] T. Hardwick,[7] G. M. Harry,[24] M. C. Heintze,[5] A. W. Heptonstall,[6] J. Hough,[9] R. Jones,[9] S. Kandhasamy,[5] S. Karki,[4] M. Kasprzack,[7] S. Kaufer,[3,15] R. Kennedy,[16] N. Kijbunchoo,[25] W. Kim,[11] E. J. King,[11] P. J. King,[1] J. S. Kissel,[1] W. Z. Korth,[6] G. Kuehn,[3,15] M. Landry,[1] B. Lantz,[17] M. Laxen,[5] J. Liu,[26] N. A. Lockerbie,[27] M. Lormand,[5] M. MacInnis,[2] D. M. Macleod,[19] S. Márka,[13] Z. Márka,[13] A. S. Markosyan,[17] E. Maros,[6] P. Marsh,[28] I. W. Martin,[9] D. V. Martynov,[2] K. Mason,[2] T. J. Massinger,[6] F. Matichard,[6,2] N. Mavalvala,[2] R. McCarthy,[1] D. E. McClelland,[25] S. McCormick,[5] L. McCuller,[2] J. McIver,[6] D. J. McManus,[25] T. McRae,[25] G. Mendell,[1] E. L. Merilh,[1] P. M. Meyers,[29] R. Mittleman,[2] K. Mogushi,[20] D. Moraru,[1] G. Moreno,[1] C. M. Mow-Lowry,[12] G. Mueller,[10] N. Mukund,[30] A. Mullavey,[5] J. Munch,[11] T. J. N. Nelson,[5] P. Nguyen,[4] L. K. Nuttall,[19] J. Oberling,[1] M. Oliver,[14] P. Oppermann,[3,15] Richard J. Oram,[5] B. O'Reilly,[5] D. J. Ottaway,[11] H. Overmier,[5] J. R. Palamos,[4] W. Parker,[5] A. Pele,[5] S. Penn,[31] C. J. Perez,[1] M. Phelps,[9] V. Pierro,[32] I. M. Pinto,[32] M. Pirello,[1] M. Principe,[32] L. G. Prokhorov,[33] O. Puncken,[3,15] V. Quetschke,[34] E. A. Quintero,[6] H. Radkins,[1] P. Raffai,[35] K. E. Ramirez,[34] S. Reid,[27] D. H. Reitze,[6,10] N. A. Robertson,[6,9] J. G. Rollins,[6] V. J. Roma,[4] C. L. Romel,[1] J. H. Romie,[5] M. P. Ross,[36] S. Rowan,[9] K. Ryan,[1] T. Sadecki,[1] E. J. Sanchez,[6] L. E. Sanchez,[6] V. Sandberg,[1] R. L. Savage,[1] D. Sellers,[5] D. A. Shaddock,[25] T. J. Shaffer,[1] B. Shapiro,[17] D. H. Shoemaker,[2] B. J. J. Slagmolen,[25] B. Smith,[5] J. R. Smith,[37] B. Sorazu,[9] A. P. Spencer,[9] K. A. Strain,[9] D. B. Tanner,[10] R. Taylor,[6] M. Thomas,[5] P. Thomas,[1] K. A. Thorne,[5] E. Thrane,[38] K. Toland,[9] C. I. Torrie,[6] G. Traylor,[5] M. Tse,[2] D. Tuyenbayev,[34] G. Vajente,[6] G. Valdes,[7] A. A. van Veggel,[9] S. Vass,[6] A. Vecchio,[12] P. J. Veitch,[11] K. Venkateswara,[36] G. Venugopalan,[6] T. Vo,[8] C. Vorvick,[1] M. Walker,[37] R. L. Ward,[25] J. Warner,[1] B. Weaver,[1] R. Weiss,[2] P. Weßels,[3,15] B. Willke,[3,15] C. C. Wipf,[6] J. Worden,[1] H. Yamamoto,[6] C. C. Yancey,[39] Hang Yu,[2] Haocun Yu,[2] L. Zhang,[6] M. E. Zucker,[2,6] and J. Zweizig[6]

(The LIGO Scientific Collaboration Instrument Science Authors)

[1]*LIGO Hanford Observatory, Richland, Washington 99352, USA*
[2]*LIGO, Massachusetts Institute of Technology, Cambridge, Massachusetts 02139, USA*
[3]*Max Planck Institute for Gravitational Physics (Albert Einstein Institute), D-30167 Hannover, Germany*
[4]*University of Oregon, Eugene, Oregon 97403, USA*
[5]*LIGO Livingston Observatory, Livingston, Louisiana 70754, USA*
[6]*LIGO, California Institute of Technology, Pasadena, California 91125, USA*
[7]*Louisiana State University, Baton Rouge, Louisiana 70803, USA*
[8]*Syracuse University, Syracuse, New York 13244, USA*
[9]*SUPA, University of Glasgow, Glasgow G12 8QQ, United Kingdom*
[10]*University of Florida, Gainesville, Florida 32611, USA*
[11]*OzGrav, University of Adelaide, Adelaide, South Australia 5005, Australia*
[12]*University of Birmingham, Birmingham B15 2TT, United Kingdom*
[13]*Columbia University, New York, New York 10027, USA*
[14]*Universitat de les Illes Balears, IAC3—IEEC, E-07122 Palma de Mallorca, Spain*
[15]*Leibniz Universität Hannover, D-30167 Hannover, Germany*
[16]*The University of Sheffield, Sheffield S10 2TN, United Kingdom*
[17]*Stanford University, Stanford, California 94305, USA*
[18]*California State University, Los Angeles, 5151 State University Drive, Los Angeles, California 90032, USA*
[19]*Cardiff University, Cardiff CF24 3AA, United Kingdom*
[20]*The University of Mississippi, University, Mississippi 38677, USA*

[21]*Instituto Nacional de Pesquisas Espaciais, 12227-010 São José dos Campos, São Paulo, Brazil*
[22]*Canadian Institute for Theoretical Astrophysics, University of Toronto, Toronto, Ontario M5S 3H8, Canada*
[23]*University of Michigan, Ann Arbor, Michigan 48109, USA*
[24]*American University, Washington, DC 20016, USA*
[25]*OzGrav, Australian National University, Canberra, Australian Capital Territory 0200, Australia*
[26]*OzGrav, University of Western Australia, Crawley, Western Australia 6009, Australia*
[27]*SUPA, University of Strathclyde, Glasgow G1 1XQ, United Kingdom*
[28]*University of Washington Bothell, 18115 Campus Way NE, Bothell, Washington 98011, USA*
[29]*University of Minnesota, Minneapolis, Minnesota 55455, USA*
[30]*Inter-University Centre for Astronomy and Astrophysics, Pune 411007, India*
[31]*Hobart and William Smith Colleges, Geneva, New York 14456, USA*
[32]*University of Sannio at Benevento, I-82100 Benevento, Italy and INFN, Sezione di Napoli, I-80100 Napoli, Italy*
[33]*Faculty of Physics, Lomonosov Moscow State University, Moscow 119991, Russia*
[34]*The University of Texas Rio Grande Valley, Brownsville, Texas 78520, USA*
[35]*Institute of Physics, Eötvös University, Pázmány P. s. 1/A, Budapest 1117, Hungary*
[36]*University of Washington, Seattle, Washington 98195, USA*
[37]*California State University Fullerton, Fullerton, California 92831, USA*
[38]*OzGrav, School of Physics & Astronomy, Monash University, Clayton 3800, Victoria, Australia*
[39]*University of Maryland, College Park, Maryland 20742, USA*

(Received 11 July 2018; published 20 February 2019)

The Advanced LIGO detectors have recently completed their second observation run successfully. The run lasted for approximately 10 months and led to multiple new discoveries. The sensitivity to gravitational waves was partially limited by laser noise. Here, we utilize auxiliary sensors that witness these correlated noise sources, and use them for noise subtraction in the time domain data. This noise and line removal is particularly significant for the LIGO Hanford Observatory, where the improvement in sensitivity is greater than 20%. Consequently, we were also able to improve the astrophysical estimation for the location, masses, spins, and orbital parameters of the gravitational wave progenitors.

DOI: 10.1103/PhysRevD.99.042001

I. INTRODUCTION

Advanced LIGO's [1] detections of gravitational waves [2–8] have opened up a new view of the Universe, allowing us to learn about astrophysical sources such as the mergers of compact stellar remnants. As work continues toward reaching the design sensitivity of Advanced LIGO, we are looking forward to more detections of gravitational waves (GW) and learning more about their sources [9,10].

The Advanced LIGO detectors are kilometer-scale laser interferometers with suspended test masses, sophisticated seismic isolation systems, and complex optical configurations employing multiple coupled optical resonators [11]. LIGO's design sensitivity is limited primarily by fundamental noise sources such as quantum shot noise, quantum radiation pressure noise, and Brownian thermal noise. However, in some frequency bands, Advanced LIGO's first observation runs have been limited by technical noises [12,13]. Many of these noise sources are well understood, and further work is needed to prevent them from contaminating the gravitational wave sensitivity. In practice, a balance has to be struck between commissioning the detector to improve noise performance, and observations. For the second observation run from November 2016 to August 2017, the LIGO Scientific Collaboration elected to run with somewhat elevated noise in one of the interferometers, while making plans to address these noise sources prior to the third observation run.

The sensitivity of the LIGO Hanford detector is severely affected by laser noise in the frequency band from 100 Hz to 1 kHz. Fortunately, we have a set of independent witness sensors that is highly correlated with this noise. The spectra of both detectors also reveal the power mains and their harmonics, as well as lines that are monitoring the calibration in real time. Noise and line removal can enhance the sensitivity of the LIGO Hanford detector by more than 20% during the second observing run. By implementing a postprocessing noise removal algorithm, we are able to significantly improve our ability to estimate the parameters of a compact binary coalescence, including its sky location, distance, masses, spins, and orbital mechanics.

The removal of lines with narrow frequency spread is also beneficial in the search for continuous wave sources, such as spinning neutron stars. Due to the long signal duration, the frequency of the observed gravitational wave

*jenne@caltech.edu

signals is Doppler shifted by the rotation of the Earth by 10^{-6} times the source-frame GW frequency and the motion of the Earth around the Sun by 10^{-4} times the source-frame frequency. Narrow spectral lines are broadened by similar ratios after the Doppler effect has been removed by projecting the data to the solar system barycenter. Additionally, lines such as the 60 Hz power mains are spectrally narrow on a short timescale but drift in frequency on a timescale of days or weeks such that when averaged over an entire observing run they obscure a span of frequencies about 0.2 Hz wide [14]. The search for continuous waves examines frequency bins as narrow as 10^{-8} Hz and is fundamentally a postprocessing algorithm so it can naturally benefit from any sensitivity improvements made via our postprocessing noise and line removal technique.

Section II briefly describes the origin of several noise sources that can be removed, while Sec. III discusses the available witness sensors and the method for calculating the coupling functions used in the subtraction algorithm. Section IV examines how this postprocessing noise subtraction impacts the estimation of various astrophysical parameters.

II. TECHNICAL NOISE SOURCES

After the first Advanced LIGO observing run, lasting from September 2015 to January 2016, the two LIGO observatories in Hanford, Washington, and Livingston, Louisiana, underwent a series of upgrades [13]. The Hanford observatory focused on increasing the amount of laser power circulating in the interferometer, which required using a high power oscillator [15]. The water required for cooling the laser rods flows through piping attached to the laser table, causing vibrations. This table also hosts an optical train for shaping the beam, impressing radio frequency sidebands, beam steering, and frequency stabilization. The water flow causes vibrations of these optical elements, which translates into beam jitter. Thermal fluctuations in the laser rods and mode mismatch in the optical resonators also cause jitter variations of the laser beam size—likely due to the turbulent water flow directly over the laser rods [16].

During Advanced LIGO's second observing run, it was discovered that one of the core mirrors in the long arm cavities at the Hanford observatory has a point absorber on its surface. Depending on the incident power, this causes a beam deformation due to the thermal expansion of the optics and the temperature dependence of the index of refraction. LIGO has a thermally actuated adaptive optics system [17] to help compensate for effects that are axially symmetric about the beam axis, but which cannot remove the effect of a point absorber that is located several millimeters away from the center.

The presence of this nonasymmetric optical deformation couples beam jitter and beam size variations into the gravitational wave readout channel. During the run, an attempt was made to inspect the offending mirror and try to clean off the absorption spot. But, this failed, with the cleaning having no appreciable effect on the absorption, so this optic has been replaced prior to the start of the third observing run. As a result, the higher beam jitter and beam size variations significantly impacted the gravitational wave readout sensitivity of the LIGO Hanford Observatory during the entire second observation run.

The LIGO Livingston Observatory did not utilize their high power laser oscillator during the second observation run, and so required much less cooling water to flow through the piping on the laser table. Instead, the commissioning effort at the Livingston Observatory focused on finding and mitigating various noise sources, such as scattered light and coupling of electronics noise. This complementary approach in the commissioning of the two LIGO detectors is common, and enables early experience with new hardware configurations. Both interferometers are susceptible to the power mains that show up in the gravitational wave readout. An active set of calibration lines is used to track the variations in the optical gain. Both the power mains and the calibration line are well known, and therefore can be subtracted from the measured gravitational wave strain.

At frequencies below a few tens of hertz, additional noise is introduced by the control forces that are applied to the mirrors to control the resonance condition of the interferometer and the test mass orientation. In addition to the 4 km long arm cavities, the LIGO detectors have optical cavities in the central part of the interferometer whose lengths must be controlled to keep the interferometer at its linear operating point. The sensors used for the auxiliary length degrees of freedom (d.o.f.) have worse shot-noise-limited sensitivity than the gravitational wave readout channel. Since this shot noise is imposed on the actual length noise of the auxiliary cavities by our feedback controls, it can contaminate the gravitational wave readout channel. The feedback control system actively tries to decouple two of the three length d.o.f. from the gravitational wave readout channel. But, due to a remaining imbalance in the actuator strength and due to leaving the third d.o.f. untouched, some noise still couples into the gravitational wave readout channel. This noise can also be removed in postprocessing.

Figure 1 shows the noise amplitude spectral density (ASD) of the LIGO detectors in the low-latency readout, and estimates the noise contributions from each of the categories described above.

III. NOISE SUBTRACTION

We use the Wiener method [18] to estimate the coupling function between each noise source and the GW channel. This method determines how best to manipulate an auxiliary witness sensor's data such that when it is subtracted from the primary target signal (here, the GW channel) the mean-square error of the primary channel is minimized. To do this, we define an error signal

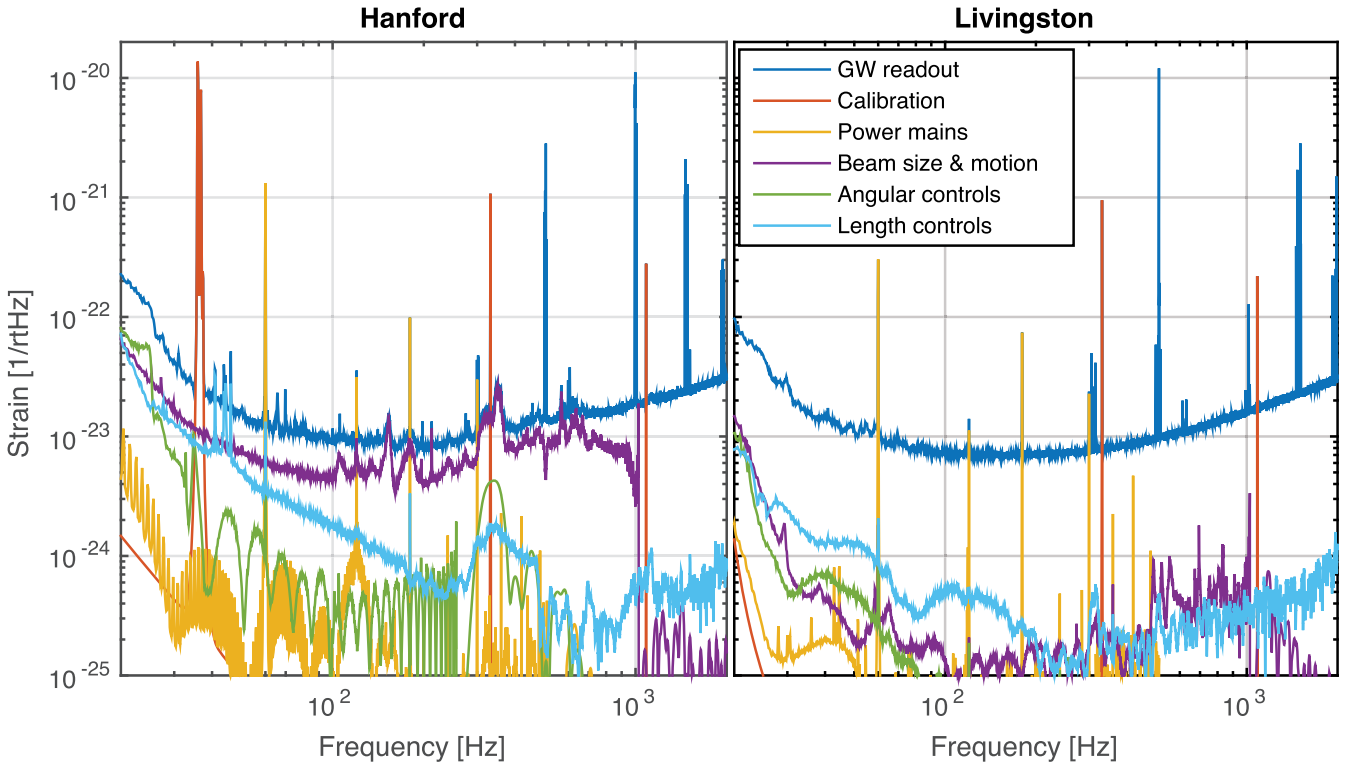

FIG. 1. Noise amplitude spectral density of the Advanced LIGO detectors (dark blue), with the left panel for Hanford and the right panel for Livingston. The other traces are the estimated contributions of the calibration lines (red), power line and harmonics (gold), beam jitter motion and beam size variations (purple), angular control noise (green), and the auxiliary length controls d.o.f. (light blue). These spectra are based on 1024 s of data starting on 25 June 2017 at 08:00:00 UTC, at a time when both LIGO interferometers were operating and in an observation-ready state.

$$\vec{e} = \vec{d} - \vec{y}, \tag{1}$$

where $\vec{d}$ is the noisy target signal and $\vec{y}$ is the approximation of $\vec{d}$ from the independent witness sensor. This is given by

$$\vec{y} = \vec{w}^{\mathrm{T}}\vec{x}, \tag{2}$$

where $\vec{x}$ is the measurement of the external disturbance from the witness sensor, and $\vec{w}$ is the finite impulse response (FIR) filter that we will solve for. The figure of merit (ξ) that we use for calculating the Wiener filter coefficients in this case is the expectation value of the square of the error signal,

$$\xi \equiv E[\vec{e}^2] = E[\vec{d}^2] - 2\vec{w}^{\mathrm{T}}\vec{p} + \vec{w}^{\mathrm{T}}R\vec{w}. \tag{3}$$

Here, $E[*]$ indicates the expectation value of $*$, $\vec{p}$ is the cross-correlation vector between the witness and target signals, and R is the autocorrelation matrix for the witness channels. When we find the extrema of Eq. (3) by setting

$$\frac{d\xi}{dw_i} = 0, \tag{4}$$

we find

$$R\vec{w}_{\mathrm{optimum}} = \vec{p}. \tag{5}$$

Equation (5) finds the time domain filter coefficients which minimize the RMS of the error $\vec{e}$ by estimating the transfer function between the witness sensors and the target signal. The error signal is now an estimate of the signal in $\vec{d}$, without any noise.

This method was utilized on LIGO data in 2010, for low frequency seismic noise [19]. Following this, the method was used to create feed forward filters which were used online in 2010 [20]. This and another method were also used offline to remove noise from auxiliary d.o.f. from LIGO's initial-era sixth science run [21,22]. A frequency-dependent variant of noise subtraction was proposed in 1999 [23], and shown to be effective on a prototype interferometer's data.

The Wiener method is able to handle several witness sensors simultaneously by extending R and $\vec{p}$ in the above equations, even if they see some amount of signal from the same noise source, as long as the information in the auxiliary sensors is not identical. This prevents over-subtracting a source of noise, and eliminates the need to carefully choose the order of subtraction if the witness sensors are used in series. The inversion of the matrix [R^{-1} when Eq. (5) is solved for $\vec{w}_{\mathrm{optimum}}$] is computationally intensive.

As this method works to minimize the root mean square (RMS) of the target channel, it is useful to remove narrow spectral lines from the data before attempting to subtract the broadband noise sources. For the calibration lines we use the digital signals that are sent to the various actuators as our auxiliary channels. Since we know that these signals sent to different actuators are not correlated with one another, we subtract them in series. For the power main line at 60 Hz we use a digitized signal that comes directly from monitoring the voltage supplied to our analog electronics racks. While we monitor the voltage at all locations that host analog electronics for the interferometer, we empirically choose the one signal at each site that removes most of the 60 Hz line. In the future, we may consider utilizing more of these signals, particularly for subtraction over longer periods of time.

To measure the beam jitter motion we use a set of three split photodiodes, each with four sections. One of the photodiodes is placed on the laser table, and monitors the beam motion and beam size just after the laser itself. This diode has a central circle, and a ring of three equal-sized segments surrounding the central region. The other two split photodetectors monitor the vertical and horizontal motion of the beam rejected by the input mode cleaner cavity which spatially filters the laser beam before it enters the main interferometer. The signals from these photodiodes are all passed to the Wiener filter calculation algorithm together.

For both the angular and length control noise sources we use the digital control signals that are sent to the mirror actuators as the witnesses.

Figure 2 shows the improvement that can be made in the LIGO interferometers' noise ASD, as a function of frequency. Note that the LIGO Hanford detector is

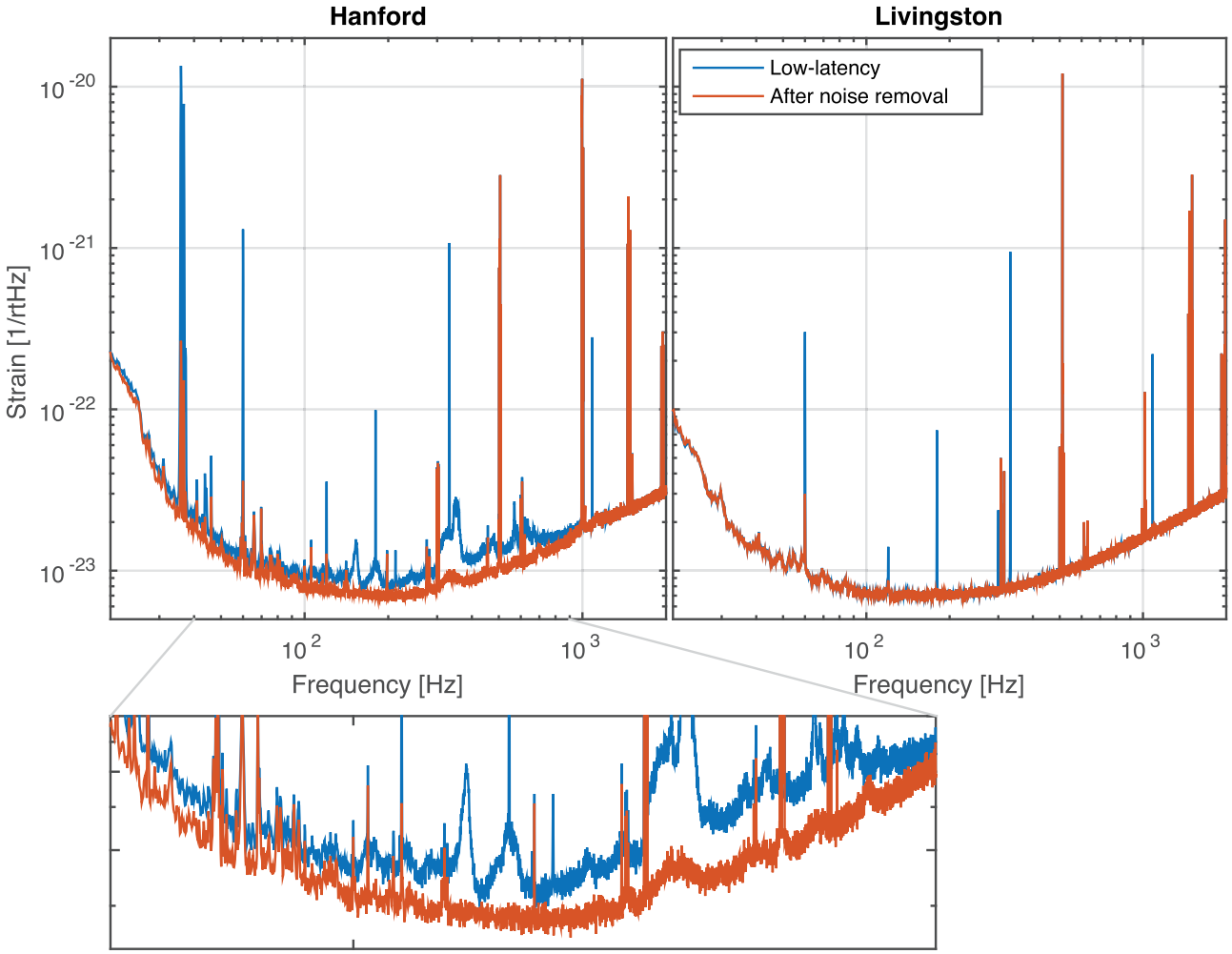

FIG. 2. Noise amplitude spectral density improvement of the LIGO detectors, Hanford in the left panel and Livingston in the right panel. Low-latency data used to identify GW candidates and determine their significance are shown in blue traces. Interferometer noise ASD after postprocessing noise removal is shown in red traces. The inset is a zoom of Hanford data. These spectra were estimated using 1024 s of data starting on 25 June 2017 at 08:00:00 UTC, a time when both LIGO interferometers were online and in an observation-ready state.

compromised by the technical noise sources discussed above more significantly than is the LIGO Livingston detector, and so it sees much more dramatic improvement. Notable spectral lines such as those at ∼500 Hz and harmonics cannot be independently witnessed with currently existing hardware, and so cannot be subtracted. The LIGO interferometers' alignment can change slowly with time, which causes the coupling of some noise sources to change. Empirically, it seems that the coupling functions should be recalculated about once per hour of data, and thus the Wiener filters are recalculated for each GW event. For all of the gravitational wave events that have utilized this method of postprocessing noise subtraction (GW170608 [8], GW170814 [7], and GW170817 [3]), the Wiener filter coupling functions were calculated using 1024 s of data, and applied in the time domain to 4096 s of data surrounding each event. The Wiener filters for each witness channel utilize 1000 finite infinite response (FIR) taps for data at a 16 kHz sample rate.

A measure of the improvement in each interferometer can be summarized by the increase in horizon distance the detectors can see a certain GW signal with a predefined signal-to-noise ratio (SNR). For both canonical binary black hole 30 $M_\odot$-30 $M_\odot$ mergers, as well as canonical neutron star 1.4 $M_\odot$-1.4 $M_\odot$ coalescences with a signal-to-noise ratio of 8, the Hanford detector improves by more than 20% while the Livingston interferometer only improves by about 0.5% using this measure.

Several checks can be done to confirm that this noise removal procedure does not affect any gravitational wave signal present in the data. Most of the noise sources have no possibility of containing any gravitational wave information, and therefore cannot remove any actual signal. For example, the power main monitors, calibration lines, and beam motion photodiodes are not directly sensitive to GWs. The witness sensor that is most sensitive to GW signals is the length of the short Michelson. We calculate that the GW signal there is a factor of 1.2×10^{-5} smaller than in the main GW readout channel [21,24,25], so it should only impact the GW signal up to 0.0012%, which we consider negligible. In Sec. IV we also examine software injected signals, where we know the true (simulated) astrophysical parameters, and can compare the estimated parameters from the low-latency data and the postprocessed noise-subtracted data.

IV. ESTIMATION OF ASTROPHYSICAL PARAMETERS

Improved interferometer sensitivity not only enhances our confidence that a signal is of astrophysical origin, but it greatly improves our ability to estimate astrophysical parameters associated with the source of the GWs.

To estimate quantitatively the impact of postprocessing noise subtraction on the characterization of GW sources, we performed software injections of signals emitted from compact binary coalescences. By software injection one means a simulated GW signal which is added to either real or synthetic interferometric noise.

For this study, we created 10 binary black hole (BBH) signals and 9 binary neutron star (BNS) signals. For the BBH, we used the `IMRPhenomPv2` waveform model, whereas for the BNS we used `TaylorF2`. This latter does not include merger and ringdown, which is a reasonable approximation at low masses. The BBH have component (detector-frame) masses randomly drawn from the range $[28-64]M_\odot$, resulting in mass ratios [26] in the range 0.48–1.0. The BBH are injected with zero spin (although we *do* allow for the spin d.o.f. while measuring the BBH parameters). The BNS have masses in the range $[1.41-1.45]M_\odot$ and no spins. The luminosity distance of the events is random in comoving volume. In practice, this results in distances between 70 Mpc and 1.54 Gpc for the BBH and 14 Mpc and 138 Mpc for the BNS.

For each signal, we add the signal offline to a stretch of the LIGO Hanford and Livingston detectors' data when both instruments were online and in a nominal observational state (1024 s beginning at 25 June 2017 08:00:00 UTC). For each signal and each instrument, a frame file (this is the file format commonly used within the LIGO-Virgo Collaboration to store GW data) containing the signal and the original noise is created and saved. The cleaning procedure is then performed on all frame files, and new "cleaned" frames are stored. This leaves us with two sets of frame files: one with the original LIGO data (as well as the GW signal), and one with the cleaned data (and, again, the signal).

Both sets of frames are analyzed with the same algorithm used by the LIGO and Virgo Collaborations to characterize compact binary coalescence sources, `LALInference` [27]. For each signal, we aim to obtain a posterior distribution for the unknown parameters on which it depends, $\vec{\theta}$, given the stretch of data containing the ith signal: $p(\vec{\theta}|d_i)$. Using Bayes' theorem, this can be written as

$$p(\vec{\theta}|d_i) \propto p(d_i|\vec{\theta})p(\vec{\theta}), \tag{6}$$

where the proportionality coefficient just acts as an overall normalization. The first term on the right-hand side, $p(d_i|\vec{\theta})$, is the likelihood of the data given the parameters. In this paper we work with a two-detector network. Assuming noise is statistically independent in the two instruments, we can write the network likelihood as the product of the likelihood in each instrument:

$$p(d_i|\vec{\theta}) = \prod_{k=1}^{\mathrm{N\,IFO}} p(d_i^k|\vec{\theta}). \tag{7}$$

Finally, $p(\vec{\theta})$ is the prior distribution of $\vec{\theta}$. For this study we used the same priors already utilized by the LIGO and Virgo Collaborations; see e.g., Ref. [28].

Most of the unknown parameters are common to both the BBH and the BNS analyses. These include component masses, luminosity distance, orbital inclination and polarization, sky position, arrival time, and phase [28]. The only difference is that for the BNS analysis we assumed spins are aligned with the orbital angular momentum, while for the BBH we allowed for the possibility of misalignment, and hence precession. For the BBH runs, we relied on the reduced order quadrature approximation to the likelihood [29] to reduce the runtime.

On average, we observe an increase of the SNR at Hanford of ∼29% for both BNS and BBH. This results in a ∼10% increase in the *network* SNR. The improvement in the network SNR is less dramatic, since the SNRs at each interferometer are added in quadrature [27].

The increased SNR at Hanford yields a more balanced distribution of the SNR across the two sites, which mostly helps measure the location of the source on the sky. For the BNS simulations, we find a 32.2% reduction of the 90% credible interval in the sky localization, compared to what was obtained with the original uncleaned data. This is shown in Fig. 3 for the loudest BNS we simulated [30]. The green curves refer to the analysis using the original data, whereas the blue curves are obtained with the cleaned data. Note that 50% and 90% contours are given, and the star shows the true position. For this BNS, the 90% sky area decreases from 39.6 deg^2 to 11.6 deg^2 using cleaned data, while the SNR in Hanford increases from 25.5 to 33.0 (the network SNR increases from 65.0 to 68.5). For BBH, the average reduction of the 90% sky uncertainty is 19.5%. The estimation of the sources' luminosity distance is also improved, although not dramatically so, since its measurement requires detection of both GW polarizations, whereas the two LIGO sites have nearly aligned arms. Adding more SNR in Hanford thus does not add significant polarization information. We find an average improvement of 6.6% for BNS and 2.0% for BBH for luminosity distance.

The intrinsic parameters of the sources, i.e., masses and spins, can usually be measured well already with a single instrument. The uncertainty in those quantities is thus mostly affected by the network SNR, and not so sensitive to how that SNR is distributed in the network. For the chirp mass [28] we find a relative improvement of 5.2% for the BNS and 13.4% for the BBH. The reason why BBH improve more is because they have fewer inspiral cycles (from which the chirp mass is measured [28]) than BNS. They can thus benefit more from any extra SNR at frequencies below ∼100 Hz.

Similar small improvements are visible for the asymmetric mass ratio and the effective spin parameter $\chi_{\rm eff}$ [28,31]. We find that cleaning makes little difference in this case. For a few BNS sources the uncertainty is actually slightly smaller before cleaning. On average, the mass ratio is estimated to be 1.4% *worse* when using cleaned data. For BBH, we also find a few sources for which the uncertainty is smaller before cleaning, although when averaging over all sources, cleaned data yield intervals which are 5.1% better with cleaned data. For $\chi_{\rm eff}$ we find an average improvement of 8.5% for BBH and 0.1% for BNS.

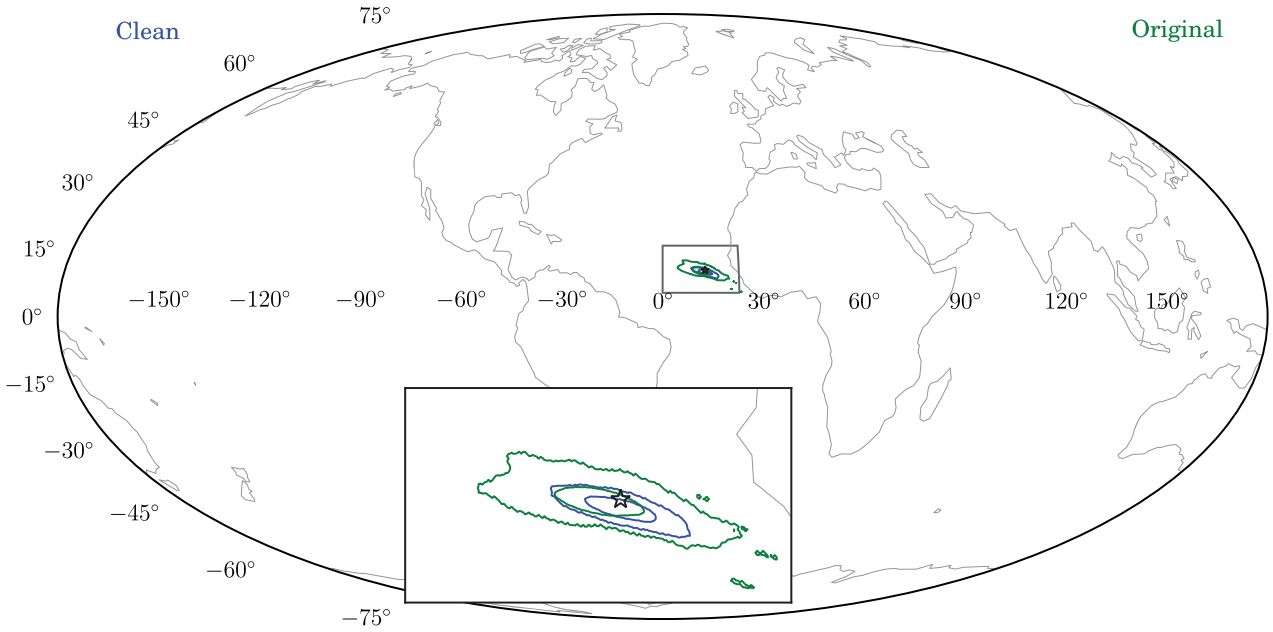

FIG. 3. Mollweide projection for the skymap of one of the BNS sources as measured with the original (green) and cleaned (blue) data. For each map the contours show the 50% and 90% confidence intervals. A star shows the true position of the injected source. To enhance clarity, the inset shows a zoom of the relevant part of the sky. The 90% confidence interval decreases from 39.7 deg^2 to 11.6 deg^2 after data are cleaned.

V. CONCLUSIONS

We have shown that postprocessing noise subtraction is effective for the Advanced LIGO gravitational wave detectors, particularly for the Hanford Observatory during the second observation run which is limited by known technical noise sources over a wide range of frequencies. This sensitivity improvement significantly enhances our ability to extract astrophysical information from our detected signals. The improvement in sensitivity shown roughly doubles the volume of the Universe in which the Hanford interferometer can detect gravitational waves. Currently underway is the rewriting of the noise subtraction code such that it is scalable and can be applied to the entirety of the data from the second observation run. This will allow the background estimations of events to also use cleaned data, and will enable the CW search to look at frequencies they have never been able to see before.

ACKNOWLEDGMENTS

The authors would like to thank the LIGO Scientific Collaboration's astrophysical parameter estimation group for their support. S. V. would like to thank R. Essick for providing the code to plot the sky location of sources. We are also very grateful for the computing support provided by The MathWorks, Inc. LIGO was constructed by the California Institute of Technology and Massachusetts Institute of Technology with funding from the National Science Foundation and operates under Cooperative Agreement No. PHY-0757058. This article has been given LIGO Document No. P1700260.

[1] J. Aasi *et al.* (LIGO Scientific Collaboration), Advanced LIGO, Classical Quantum Gravity **32**, 074001 (2015).
[2] B. P. Abbott *et al.* (LIGO Scientific and Virgo Collaborations), Observation of Gravitational Waves from a Binary Black Hole Merger, Phys. Rev. Lett. **116**, 061102 (2016).
[3] B. P. Abbott *et al.* (LIGO Scientific and Virgo Collaborations), GW170817: Observation of Gravitational Waves from a Binary Neutron Star Inspiral, Phys. Rev. Lett. **119**, 161101 (2017).
[4] B. P. Abbott *et al.*, Multi-messenger observations of a binary neutron star merger, Astrophys. J. Lett. **848**, L12 (2017).
[5] B. P. Abbott *et al.* (LIGO Scientific and Virgo Collaborations), GW151226: Observation of Gravitational Waves from a 22-Solar-Mass Binary Black Hole Coalescence, Phys. Rev. Lett. **116**, 241103 (2016).
[6] B. P. Abbott *et al.* (LIGO Scientific and Virgo Collaborations), GW170104: Observation of a 50-Solar-Mass Binary Black Hole Coalescence at Redshift 0.2, Phys. Rev. Lett. **118**, 221101 (2017); **121**, 129901(E) (2018).
[7] B. P. Abbott *et al.* (LIGO Scientific and Virgo Collaborations), GW170814: A Three-Detector Observation of Gravitational Waves from a Binary Black Hole Coalescence, Phys. Rev. Lett. **119**, 141101 (2017).
[8] B. P. Abbott *et al.* (LIGO Scientific and Virgo Collaborations), GW170608: Observation of a 19 solar-mass binary black hole coalescence, Astrophys. J. Lett. **851**, L35 (2017).
[9] B. P. Abbott *et al.* (KAGRA, LIGO Scientific, and Virgo Collaborations), Prospects for observing and localizing gravitational-wave transients with Advanced LIGO, Advanced Virgo and KAGRA, https://dcc.ligo.org/LIGO-P1200087/public.
[10] B. P. Abbott *et al.*, Prospects for observing and localizing gravitational-wave transients with advanced LIGO and advanced virgo, Living Rev. Relativity **19**, 1 (2016).
[11] B. P. Abbott *et al.* (LIGO Scientific and Virgo Collaborations), GW150914: The Advanced LIGO Detectors in the Era of First Discoveries, Phys. Rev. Lett. **116**, 131103 (2016).
[12] D. V. Martynov *et al.* (LIGO Scientific Collaboration), Sensitivity of the Advanced LIGO detectors at the beginning of gravitational wave astronomy, Phys. Rev. D **93**, 112004 (2016).
[13] B. P. Abbott *et al.* (LIGO Scientific and Virgo Collaborations), Supplement: GW170104: Observation of a 50-solar-mass binary black hole coalescence at redshift 0.2, https://journals.aps.org/prl/supplemental/10.1103/PhysRevLett.118.221101.
[14] B. P. Abbott *et al.* (LIGO Scientific and Virgo Collaborations), Directional Limits on Persistent Gravitational Waves from Advanced LIGO's First Observing Run, Phys. Rev. Lett. **118**, 121102 (2017).
[15] P. Kwee, C. Bogan, K. Danzmann, M. Frede, H. Kim, P. King, J. Pöld, O. Puncken, R. L. Savage, F. Seifert, P.Wessels, L. Winkelmann, and B. Willke, Stabilized high-power laser system for the gravitational wave detector advanced LIGO, Opt. Express **20**, 10617 (2012).
[16] R. Schofield, A 9% increase in crystal chiller water flow increased the HPO jitter signal at the DBB and in DARM by 25% at 450 Hz, LIGO Hanford Observatory alog number 30290, https://alog.ligo-wa.caltech.edu/aLOG/index.php?callRep=30290.
[17] A. F. Brooks *et al.*, Overview of Advanced LIGO adaptive optics, Appl. Opt. **55**, 8256 (2016).
[18] N. Wiener, *Extrapolation, Interpolation, and Smoothing of Stationary Time Series* (M.I.T. Press, Cambridge, 1964).
[19] J. C. Driggers, M. Evans, K. Pepper, and R. Adhikari, Active noise cancellation in a suspended interferometer, Rev. Sci. Instrum. **83**, 024501 (2012).
[20] R. DeRosa, J. C. Driggers, D. Atkinson, H. Miao, V. Frolov, M. Landry, J. A. Giaime, and R. X. Adhikari, Global feedforward vibration isolation in a km scale interferometer, Classical Quantum Gravity **29**, 215008 (2012).

[21] G. D. Meadors, K. Kawabe, and K. Riles, Increasing LIGO sensitivity by feedforward subtraction of auxiliary length control noise, Classical Quantum Gravity **31**, 105014 (2014).
[22] V. Tiwari, M. Drago, V. Frolov, S. Klimenko, G. Mitselmakher, V. Necula, G. Prodi, V. Re, F. Salemi, G. Vedovato, and I. Yakushin, Regression of environmental noise in LIGO data, Classical Quantum Gravity **32**, 165014 (2015).
[23] B. Allen, W. Hua, and A. Ottewill, Automatic cross-talk removal from multi-channel data, arXiv:gr-qc/9909083.
[24] J. C. Driggers, Noise cancellation for gravitational wave detectors, Ph. D. thesis, California Institute of Technology, 2015, https://thesis.library.caltech.edu/8998/.
[25] K. Izumi and D. Sigg, Advanced LIGO: length sensing and control in a dual recycled interferometric gravitational wave antenna, Classical Quantum Gravity **34**, 015001 (2017).
[26] We define the mass ratio $q \equiv m_2/m_1$, where by convention $m_1 \geq m_2$.
[27] J. Veitch *et al.*, Parameter estimation for compact binaries with ground-based gravitational-wave observations using the LALInference software library, Phys. Rev. D **91**, 042003 (2015).
[28] B. P. Abbott, R. Abbott, T. D. Abbott, M. R. Abernathy, F. Acernese, K. Ackley, C. Adams, T. Adams, P. Addesso, R. X. Adhikari *et al.*, Properties of the Binary Black Hole Merger GW150914, Phys. Rev. Lett. **116**, 241102 (2016).
[29] R. Smith, S. E. Field, K. Blackburn, C.-J. Haster, M. Pürrer, V. Raymond, and P. Schmidt, Fast and accurate inference on gravitational waves from precessing compact binaries, Phys. Rev. D **94**, 044031 (2016).
[30] Most of the other events show similar improvements; we chose to show this one because for other sources the skymap has a characterizing ringlike structure, which does not allow one to clearly see the difference between the reconstructions.
[31] É. Racine, Analysis of spin precession in binary black hole systems including quadrupole-monopole interaction, Phys. Rev. D **78**, 044021 (2008).